Chapter 4

Experimental and Numerical Studies on Imbibition

4.1 Introduction

In this chapter we study a non-equilibrium classical statistical mechanics problem by experiment and numerical simulation. The study concerns the static as well as dynamic properties of the interface formed as a result of the seepage of fluid through a random porous medium. Interface growth phenomena have been studied in a variety of systems [1, 2, 3, 4, 5]. The main interest is to understand the morphology of the interface.

The basic aim here is to study the effect of various factors in shaping the roughness of the interface. There are several kinds of interfaces in nature. Examples of the interface motion in disordered media are (1) fluid flow in porous media (2) propagation of flame fronts and (3) pinning of flux lines in High Temperature Super-conductors by random impurities. In a deposition process, one can have (i) atom deposition and (ii) roughening in Molecular Beam Epitaxy. Rough interfaces are formed in biological systems as well e.g. growth of a bacterial colony.

In this chapter, we study the interface generated by a fluid imbibed into a random porous medium. The main motivation for studying these interfaces is to understand the underlying mechanism which leads to roughening of the interface. This might help in characterizing a random medium. The roughening process is studied through

scaling. The exponents obtained under this scaling are independent of 'many' details of the system. This allows one to understand the roughness of the interface of different systems even though these systems differ in the detailed mechanism by which the interface is formed. From the point of view of statistical modeling, one would like to classify a large number of theoretical models developed for various contexts into a small number of universality classes.

The various sections of this chapter are organized as follows. In section 2 we describe the imbibition process in random porous medium. After a brief introduction to characteristics of the rough interface, we critically comment on the existing models for imbibition. Then, we describe our experimental setup and the results. In section 6, we present our model to study imbibition. A numerical study of the model and comparison of the results with that of experiments is given in section 7. Self-organized criticality (SOC) and the multi-affinity in this model have also been discussed in subsequent sections. In section 10, we present a comparative study of our model with other growth models. Finally, in section 11 we give our conclusions.

4.2 Imbibition in Porous Medium

We describe here a process where a dark staining fluid is sucked into a 2D random porous medium. For example, if a paper is fixed with the bottom end dipped into a solution, then the fluid is imbibed into the pores of the paper by capillary action. An interface is formed by the wet front which rises steadily. On microscopic length scales, paper is an extremely disordered substance formed by long fibers which are randomly distributed and randomly connected [6]. The randomness present in the paper and evaporation of the fluid from the bulk of the paper tends to arrest the motion of the wetting front. The motion of the wet front is also affected by the ratio of the size of the molecules present in the solution to the pore size and viscosity of the fluid. Since evaporation takes place from the sides of the paper as the fluid rises,

the front gets dried up. The front stops moving when the fluid at the boundary has completely evaporated. Finally, a rough interface results. These experiments provide a simple laboratory system to study flow through a random porous medium. This study is of relevance to thin layer and paper chromatography. They could also provide good "table top" systems to study pattern formation [7, 8].

There are distinct qualitative differences between this interface formation in imbibition and other growth processes. For example, the rough interface in deposition process arises when particles are deposited randomly over a surface. But, the roughness of the interface in imbibition is solely due to the disorder in the paper. If there is no blocking of the pores, the interface will be smooth at any rate of evaporation. However, the disorder experienced by the fluid is indirectly affected by the evaporation. There could be many paths through the fibers of the paper to reach a particular site. When the evaporation is small, the fluid can take even longer paths to reach a site. This changes the effectiveness of the randomness of the medium making the interface rough. For the same amount of randomness, the number of paths will be less when the evaporation is higher, because higher evaporation eliminates longer paths.

4.3 Characterization of the Interface

In our experiment and simulation, a one-dimensional interface is formed by fluid flow through a 2-dimensional random porous medium.

The surface can be instantaneously described by its height $h(x)$ as a function of x, where x is a spatial coordinate. As the surface evolves in time, $h(x,\mathrm{t})$ depends on both space and time. Let us define $W(l,\mathrm{t})$, the correlation of the fluctuations in the height at two points x and x $+ l$ at a fixed time t as

$$W(l,t) = \left\langle (h(x,t) - h(x+l,t))^2 \right\rangle_x^{1/2} \tag{4.1}$$

where $\langle ... \rangle_x$ denotes an average over x. Experimental observation indicates that

W(1, t) satisfies a scaling law :

$$W(l,t) \sim l^{\alpha} f(t/l^{\frac{\alpha}{\beta}}) \tag{4.2}$$

The exponent α and β quantify the static and dynamic roughness of the interface. The two limits of the scaling function are: f (u) $\sim u^{\beta}$ for $u \ll 1$ and f (u) $\sim const.$ for $u \gg 1$. We also study the correlation function

$$C(l,\tau) = \left\langle (h(x+l,t+\tau) - h(x,t))^2 \right\rangle_{x,t}^{1/2} \tag{4.3}$$

where $\langle ... \rangle_{x,t}$ denotes an average over x as well as a time average over a time scale short compared to the relaxation time. For 1 $\ll$ L (system size) , $C(l,0) \sim l^{\alpha}$; while for short times, $C(0,\mathrm{r}) \sim \tau^{\beta}$. Note that $C(l,\mathrm{r})$ scales similarly with $W(l,t)$. In the subsequent section we denote $C(l,0)$ and $C(0,\mathrm{r})$ by W(l) and $C(\tau)$ respectively.

It is known that the roughness of the wet front can be described as a self-affine fractal [2]. Self-similar fractals are invariant under isotropic dilation while the self-affine ones are statistically invariant under an anisotropic dilation. Mathematically, the self-affine interface is invariant under the transformation x $\rightarrow$ bx and h $\rightarrow b^{a}h$ (with $a \neq 1$). This self-affinity of the interface implies a bound on the roughness exponent a. The self-affine interface looks flat when viewed at a sufficiently large length scale. This means immediately $a < 1$. In fact in our experiment as well as in simulation, we always obtain $a < 1$.

4.4 Review of Previous Work on Imbibition

In 1994, Amaral et. al. [6], in an experiment using paper towels and coffee found the roughness exponent to be $0.65 \pm .05$. They pointed out that this exponent is robust in the sense that it does not depend on the evaporation, concentration of the solution and the kind of paper used. A directed percolation depinning (DPD) model [9] was developed to study the interface roughening of interfaces in porous medium. This model is defined as follows (see figure (4.1)). On a square lattice of

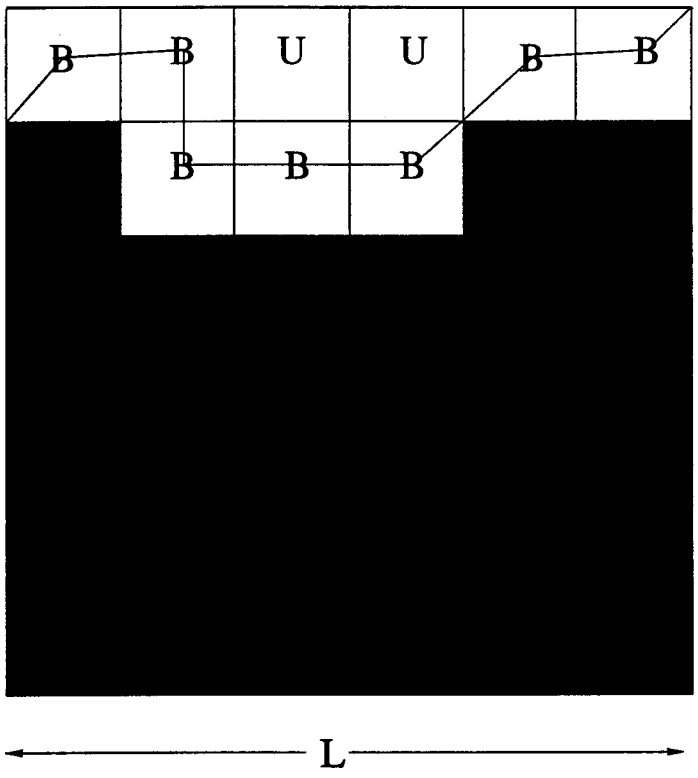

Figure 4.1: *A Schematic Diagram for Directed Percolation Model*

size L with periodic boundary condition, a fraction p of the cells is blocked (marked by 'B'). **A** blocked cell does not allow the interface to grow while the interface is allowed to advance through an unblocked cell. At $t = 0$, the bottom row is filled with fluid (shaded) and the interface is a horizontal line. At $t = 1$, one cell (say 'X') from the unblocked cells that are nearest neighbours (U-cells) to the interface is chosen randomly. This cell 'X' becomes wet; in addition, all cells (regardless of type) below it in the same column also get shaded. This process is then repeated. For p values below a critical threshold p_c, the interface propagates without stopping. While if the density of blocked cells is high enough ($p > p_c$), the interface will eventually get pinned. This happens when it meets a directed percolating string of blocked cells that runs across the lattice from left to right. To include evaporation, a variant of this DPD model was proposed [6]. In this model (DP) [6], evaporation was incorporated phenomenologically by a steady increase **(Ap)** at each time step

in the probability p of blocking the pores. Such an increase in p naturally drives the system into a percolation threshold p_c, wherein a cluster of blocked cells spanning across the system is obtained. In other words, in this model the effective density of pinning centers increases as the distance between the interface and the source increases.

Such a spanning path (see figure (4.1)) is characterized by two correlation lengths; one $(\xi_{\|})$ is parallel to the interface and the other one $(\xi_{\perp})$ is perpendicular to it. These two correlation lengths diverge with different exponents $\nu_{\|}$ and $\nu_{\perp}$ near p_c. The static exponent obtained in this [6]simulation in two dimensions was 0.63 ± 0.02. An analytical argument was given for the static exponent 0.63 obtained in numerical simulation by identifying the $\xi_{\|}(\sim (\mathrm{p} - p_c)^{-\nu_{\|}})$ with l and $\xi_{\perp}(\sim (\mathrm{p} - p_c)^{-\nu_{\perp}})$ with W [1]. Therefore,

$$W \sim \xi_{\perp} \sim |p - p_c|^{-\nu_{\perp}} \sim \xi_{\|}^{\nu_{\perp}/\nu_{\|}} \sim l^{\nu_{\perp}/\nu_{\|}} = l^{\alpha} \tag{4.4}$$

It is known [10] from numerical calculation on directed percolation in $(2+1)$ dimension that $\nu_{\|} = 1.733$ and $\nu_{\perp} = 1.097$. This immediately gives $\alpha = \nu_{\perp}/\nu_{\|} = 0.63$. A variant of the DPD model with global updating called the self-organized depinning (SOD) model has been recently developed by Sneppen [11]. In this model (SOD), the interface grows on the site at which the pinning force is the smallest. The constraint on the slopes of the height variable $(|h(y) - \mathrm{h(y-1)}| < 1)$ acts after the least pinned site is moved. The static roughness exponent in this model was found to be 0.63 ± 0.02 which is the same as that found in DPD model.

4.5 Experiment

We will now describe our experimental setup to study imbibition in porous medium. We use Whatman No:1 filter paper as the porous medium and ink as the dark

[1]This identification is valid so long as there is a single transverse characteristic length $\xi_{\perp}$ for directed percolation clusters.

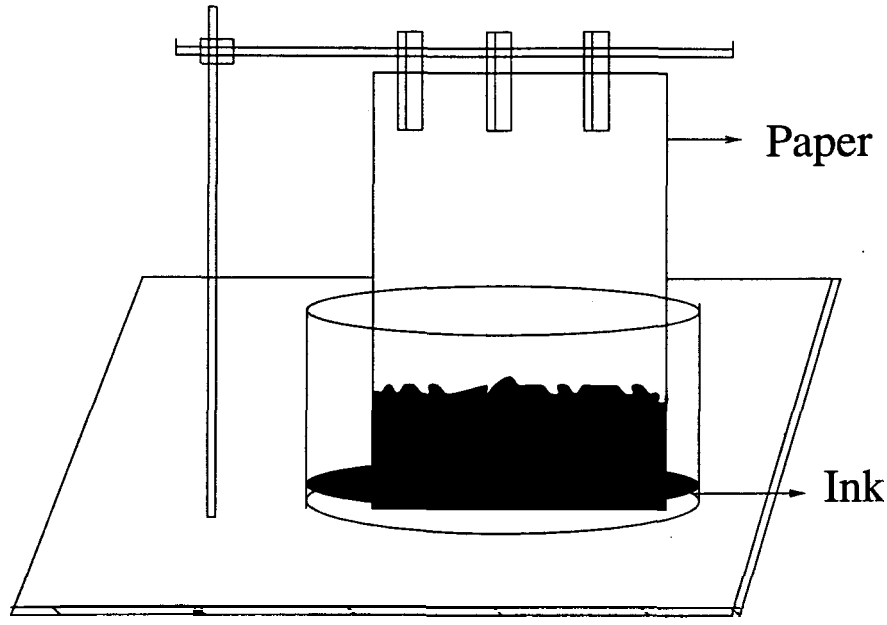

Figure 4.2: *Schematic Diagram* of *Experimental Setup (Vertical Geometry)*

staining fluid. The experiments can be carried out in two geometries as shown in figure (4.2) and figure (4.3). In figure (4.2), the paper was held vertically and the ink rises through the pores. In another geometry (figure (4.3)) , the paper was spread horizontally over a glass plate. In this case, the ink rises through the capillary tube and then spreads horizontally in the paper. As is evident here, all positions in the paper are equivalent under gravity. So, the effect of gravity drops out in this horizontal geometry. The size of the paper taken for the vertical geometry was $28.5cm \times 23$cm while for the horizontal geometry 16cm x $22cm$. We here present the experimental result [12] for the vertical geometry.

The evaporation rate was varied by changing the room humidity and temperature (by using a room air conditioner). Initially, the water front and the dye in the ink solution emerge together, but after 15-20 seconds or so the water front moves ahead of the dye front. This could be due to the fact that the organic dye molecules are larger than the water molecules. After an hour or so both the fronts again meet together and move jointly since the movement of water is now reduced considerably by evaporation. And finally, the ink stops at a particular height. The darkening

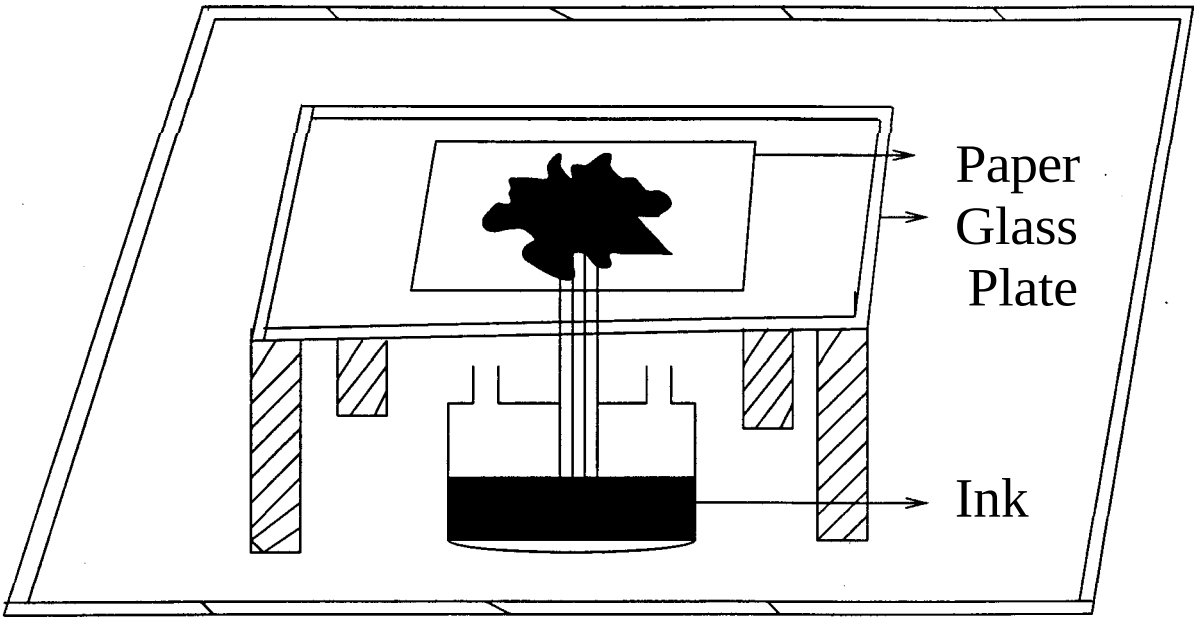

Figure **4.3:** *Schematic Diagram of Experimental Setup (Horizontal Geometry)*

of the interface indicates this stoppage of growth. This darkening is due to the following reason. As the ink rises water evaporates from the paper. As a result, the dye molecules carried by the water get deposited at the interface continuously causing a darkening of the boundary. The paper was taken out from the solution and dried when this darkening took place. The interface was photographed with a Philips CCD camera (56472 CCIR) and the image was digitized using a DT-IRIS 2851 frame grabber card. The image was analyzed using the software provided with the frame-grabber. The CCD camera has an image area 6mm. x $4.5mm.$ containing 604 x 588 pixels. We divided the horizontal length of the paper into several segments and each segment was digitized accordingly. A typical image of the interface obtained from the experiment is shown in figure (4.4(a)).

Since altering conditions in the room is found to change the roughness of the interface even after it is dried, the humidity and temperature of the room was kept constant till the image was digitized. In figure (4.4(b)), we also show the interface generated from the simulation of our model described below. Figure (4.5) shows the behaviour of $W(l)$ against l for two different values of evaporation rate. The data

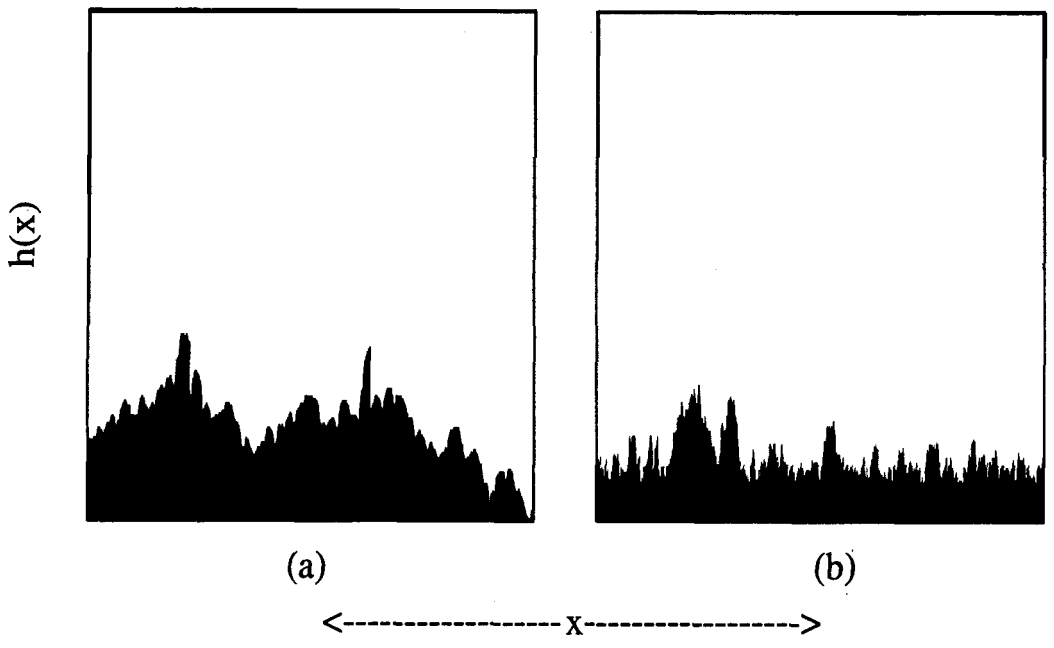

Figure 4.4: (a) *A digitized image of the interface from experimental set-up of vertical geometry. (b) A typical result of the simulation obtained using the model.*

were averaged over 10 experiments.

We find the value of a to be $.45 \pm .05$ and $.66 \pm .02$ for higher (humidity 50.0% and temperature 21.0^oC) and lower evaporation (humidity 60.0% and temperature 23.0^oC) respectively. However, we do not have a quantitative measurement of the evaporation. Thus, a is very different for the two cases.

In a recent experiment by T. H. Kwon et. al. [9] with paper-towel wetting with a red food dye solution, the static roughness exponent was found to be $0.67 \pm .04$. A dependence of a on the external parameter is also exhibited by DPD [9] models when the growth is stopped before it reaches p,. There the exponent crosses over to the Kardar-Parisi- Zhang(KPZ)[2] [14] value. The change in a shown by the experiments above is different from this crossover since we see values of a below KPZ ($a = .5$) and above DPD ($a = .63$). This shows that unlike the results of reference [6], a is not quite robust against the external parameters. Varying exponents ($0.62 - 0.78$) have also been observed in experiments by Family et. al. [15]. Notice the exponents are

[2]In its one-dimensional version, the KPZ equation reads as $\frac{\partial h}{\partial t} = \nu \nabla^2 h + \frac{\lambda}{2}(\nabla h)^2 + \zeta(x,t)$. The noise ζ has the following correlations; $< \zeta >= 0$ and $< \zeta(x,t)\zeta(x',t') >= D\delta(x-x')\delta(t-t')$.

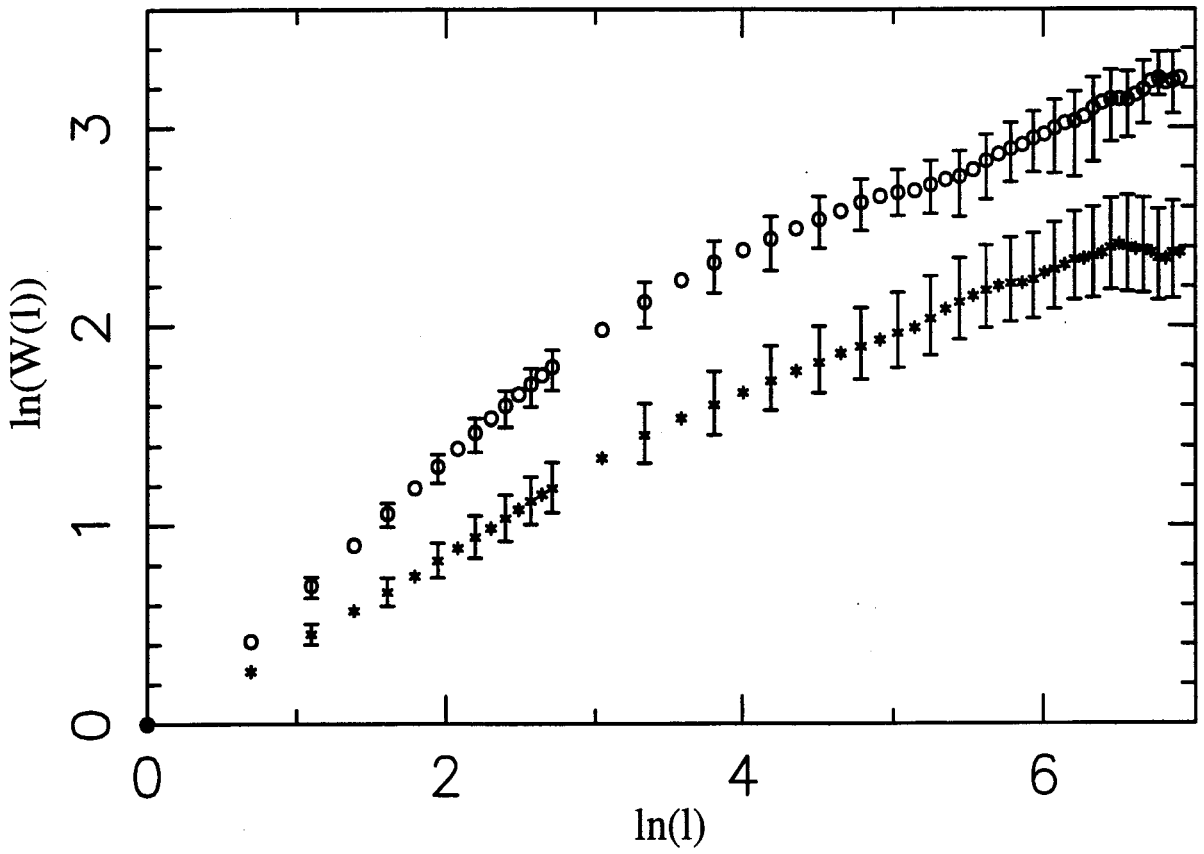

Figure **4.5:** *The experimental values of height-height correlation function $W(l)$ plotted against the distance of separation l after the interface stopped growing. Points marked with *fall onto a curve with exponent* $.45 \pm .05$. *For lower evaporation the points (marked o) correspond to an exponent* $.66 \pm .02$.

not the same as obtained from Edwards and Wilkinson Model [16] and Restricted Solid on Solid model [17]. (see Appendix B for a comparison of the exponents obtained in various experiments.)

4.6 The Cellular Automaton Model

To understand the dependence of the various parameters affecting the growth of interface in imbibition of a dark staining fluid into 2D random porous medium, we present the following model. Before discussing the model used in the simulation let us try to understand the problem from a microscopic point of view. In the experiments described above paper was used as the random medium. A paper is made of criss-crossed fibers. Ink flows both through the paper and through regions

in between the fibers. Disorder stems mainly from the random orientation and length of these fibers. This disorder in the paper does not change with time, so a quenched disorder is appropriate for the description of the theoretical model. Thus, at a microscopic level one can regard the paper as a randomly disordered medium [6] with a time independent probability p for the pores to be blocked. So, . the interface growth phenomena described here can be modeled as the propagation of fluid particles through this disordered medium. The wetting front of the fluid particles propagates due to the capillary forces. The disorder in the medium and the evaporation tend to arrest this growth. It should be noted that for $p < p_c$ (i. e. when at any given time there is a nonzero number of paths normal to the interface) this pinning is possible only when the evaporation is present.

Evaporation constantly decreases the number of fluid particles in the wetting front. This makes it more difficult for the fluid to overcome the obstacles. The front stops when the number of fluid particles goes to zero. To see it more clearly, we can associate a dimensionless internal driving force with the interface with the property that this force vanishes as the interface stops growing. The front stops moving when $f \to 0$ at a critical height. This is substantiated by the fact that in the experiments for smaller evaporation, we observe larger critical height.

In our model [12] the porous medium is considered as a square lattice with disorder being incorporated by blocking some cells randomly with a probability $p < p_c$ (see figure (4.6)). The maximum capacity of each cell is fixed to N_0 number of particles *i.e.* the cells are of fixed volume and the fluid is incompressible. At every time step, evaporation was explicitly modeled by the loss of n number of particles from a cell. At time t=0, at the bottom edge of the lattice a horizontal line of wet cells with N_0 particles is created. At $t = 1$ the particles are imbibed into all unblocked cells which are nearest neighbours to the wet region. The wet cells are however, not depleted due to replenishment from the source below. If N is the

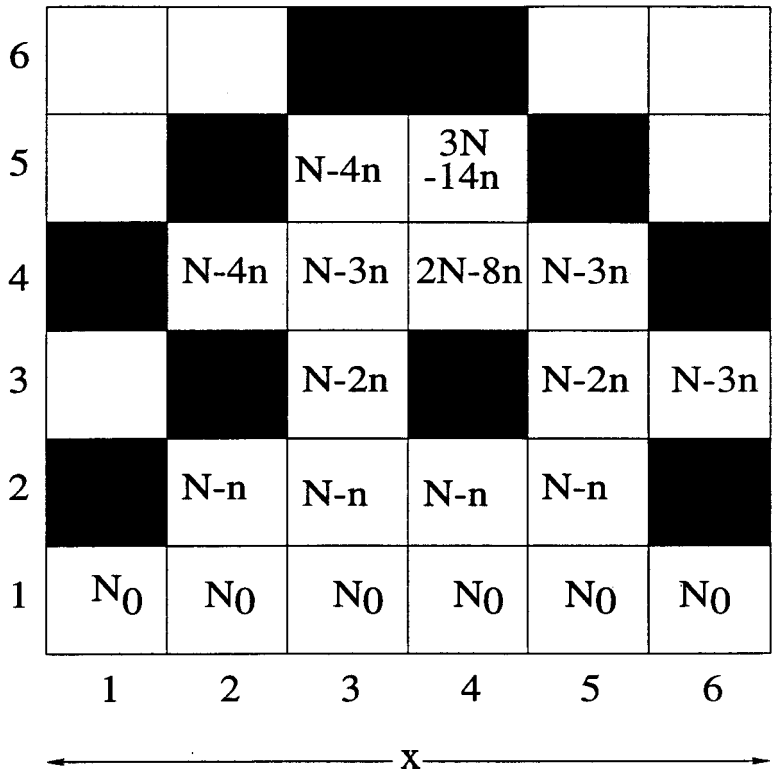

Figure 4.6: *Example of the multiple connectivity of the model for a 6X6 lattice. The blocked cells are shown black. Note that the cell (4,4) gets particles from both (4,3) and (4,5). Also when a cell* (i_s,j) *is wet all the other cells* (i,j) *with* $i < i_s$ *are wet as well.*

number of particles in a wet cell then it transfers N – n particles to all its unblocked nearest neighbours *i.e.* each of the neighbours gets N – n particles, n being the loss due to evaporation. This updating is done in parallel *i.e.* all cells which are nearest neighbours to the front are updated simultaneously. When a cell transfers to its nearest neighbours the number of particles it contains remains the same due to the replenishment from the source below. If a cell has more than one wet nearest neighbour, it gets particles from all of them subject to a maximum number N_0. We also apply the rule that every cell blocked or unblocked below a new wet cell becomes wet [6] as well with N_0 particles. This is to avoid the presence of overhangs. We use periodic boundary condition in horizontal direction x by identifying the cells at the edges of the lattice. In the vertical direction, the lattice is semi-infinite (Typical numbers: $L_x = 6000$, $N_0 = 150$, n = 20, p = .45.).

In this model, a change in concentration of the fluid can be modeled by changing the maximum allowed number of fluid particles in a cell N_0.

We can apply an external bias which could be present due to gravity or anisotropy in the medium. This bias was incorporated in the model by introducing a difference in the number of fluid particles transferred to the vertical and horizontal neighbours of a given cell.

There are two independent parameters in the model. They are (i) the blocking probability p and (ii) the ratio $\eta = n/N_0$.

The model is different from that of reference [6], in the sense that here the effect of evaporation is incorporated in an explicit way. Unlike the directed percolation model, where the interface stops only when it is pinned by a connected cluster of blocks, in our model it can also stop when the wetting front runs out of fluid due to evaporation. When this happens, a connected cluster of dry cells (which could be blocked or unblocked) forms at the boundary. It should be noted that there is no analogue of the stopping of growth in DPD model by running out of fluid. In DPD growth model, the wetting front does not stop for $p < p_c$. However, in our model for all values of evaporation, the interface stops, forming a connected cluster of dry cells.

The model is also different from Eden[3] growth [18] in the sense that all the sites in the boundary move at the same time *i.e.* here the growth process by itself does not cause interface roughness. The model can be used to study *thin* layer *chromatography* wherein a mixture of different chemical compounds are made to diffuse through a porous medium resulting in their separation.

[3] The model was originally introduced for the formation of cell colonies, such as bacteria or tissue cultures. In its prototype lattice version, a seed particle is placed at the origin. A new particle is added on any randomly chosen perimeter site of the seed, forming thereby a two site cluster. The process is iterated to generate a rough perimeter. To study the interface properties of the model, it is convenient to start the growth from an entire line of seeds instead of from a single seed.

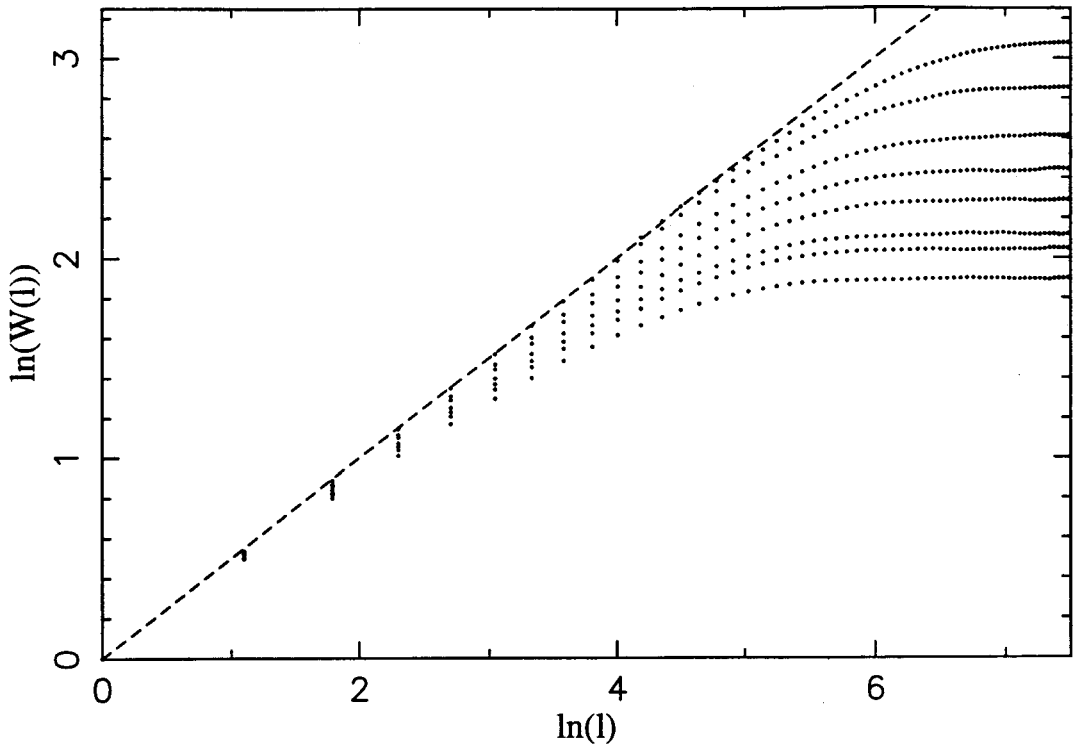

Figure *4.7: The simulated correlation function W(1) plotted against the distance of separation 1 after the columns stopped growing. The parameters are* $p = .45$, $L = 6000$ *and* $\eta = .12$ *to* .148 *in equal intervals of* .004 *from top.*

4.7 Simulation Results and Discussion

Unless specified the simulations are done on a lattice of horizontal length 6000 units. The results are averaged over *500* realizations.

4.7.1 Static and Dynamic Exponent

In figure *(4.7)* we show the behaviour of $W(l)$ as a function of l for different values of evaporation for a fixed value of p and lattice size L. The simulations show the existence of a crossover length *1,* such that the height - height correlation function $W \sim l^{a}$ for $1 \ll l_{\times}$. Whereas for $1 \gg l_{\times}$, W saturates to a constant value W_{sat}. The exponent a is a function of evaporation η while the value of W_{sat} and *1,* depend on both the system size L and evaporation η. The dependence of a and W_{sat} on evaporation is consistent with that found in the experiment as can be seen by comparing figures *(4.5)* and *(4.7).*

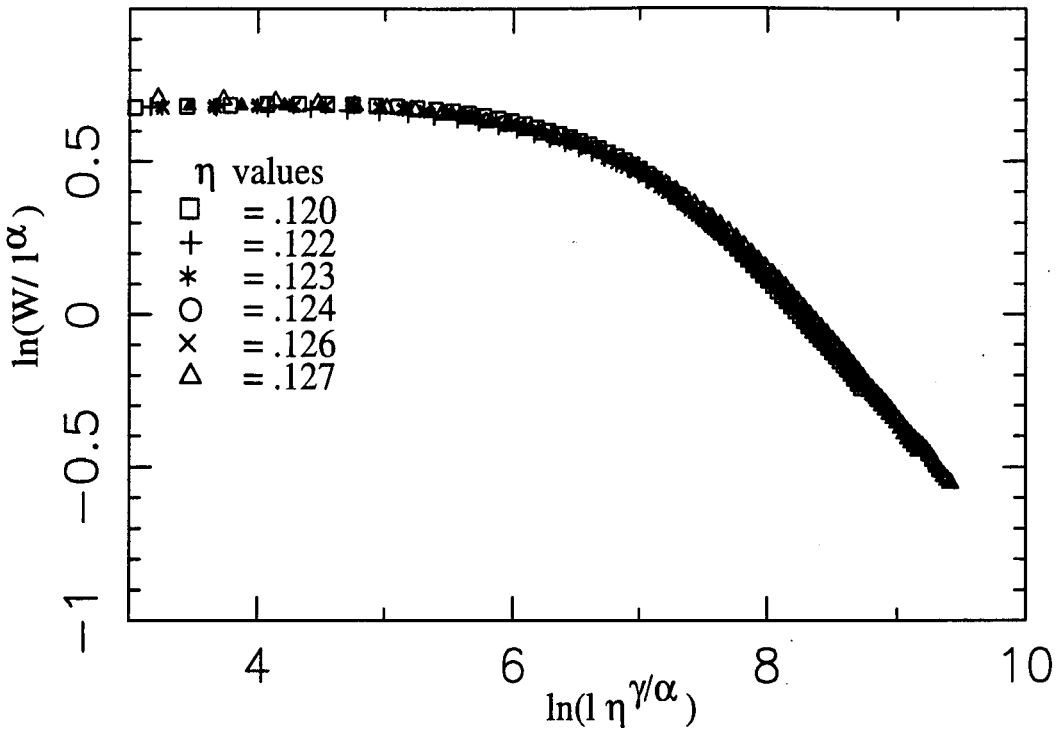

Figure *4.8: The data collapse of $W(l)$ vs l for various values of evaporation. The parameters are $p = .45$ and $L = 6000$. The x direction scale has been rescaled with respect to $N_0 = 150$. The exponent a and γ was found to be 0.5 and 3.0.*

The saturated correlation W_{sat} depends upon the evaporation η as

$$W_{sat} \sim (\eta)^{-\gamma} \tag{4.5}$$

So, in the region where a is independent of η one can obtain a scaling form (from the simulated data)

$$W(l,\eta) \sim l^{\alpha}\ f(l\ \eta^{\gamma/\alpha}) \tag{4.6}$$

where f $(x) \rightarrow const.$ *as* $x \rightarrow 0$ and $f(\mathrm{x}) \rightarrow x^{-\alpha}$ as $x \rightarrow \infty$. The data collapse is shown in figure *(4.8)*. It has been verified numerically that the scaling form *(4.6)* holds over a narrow range of evaporation (η ranges from .134 to .147) with exponents a depending explicitly on evaporation.

We will see how the height - height correlation exponent a changes with time. This is depicted in figure *(4.9)*. At short times (transient regime) α shows a rapid increase. At late times a saturates to a value α_{sat} which depends on evaporation. This establishes the fact that the roughness of the interface is controlled by evaporation and that the reason for the dependence of α on η is not due to the lack of

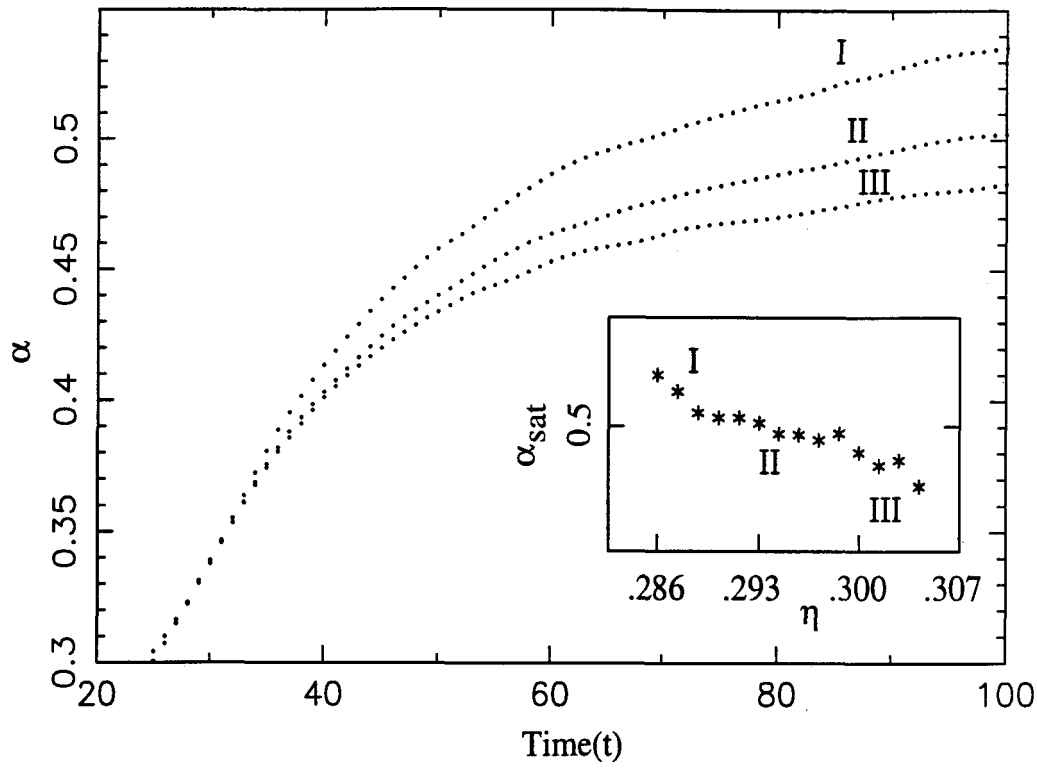

Figure 4.9: *The growth of exponent a as a function of time for p = .2 and L = 6000. The three regimes are marked I, II and III. The lines are for* η = .286, .295, .300 *respectively. The behaviour of* α_{sat} *with evaporation* η *in this three regime is shown in the inset.*

time for the interface to saturate.

We find that there are two critical values[4] of evaporation η_1 and η_2 (see figure (4.9)). For low values of evaporation the mean height increases without stopping (regime I). Above the critical evaporation η_1 (regime II) the mean height stops after a finite time. We find in this region ($\eta_1 < \eta < \eta_2$) a $= 0 \cdot 5$ and $\gamma = 3.0$. Note that this value is not the same as the exponent obtained in DPD simulation. The scaling plot shown in figure (4.8) is in this region. Above the second critical evaporation rate η_2, this scaling breaks down. For $\eta > \eta_2$ (regime 111), the exponent a decreases continuously with η as can be seen from the inset of figure (4.9). For p = .45, we obtain $\eta_1 = .124$ and $\eta_2 = .134$. And for p = .2, we get higher values of η_1 and η_2 as is seen from the inset of figure (4.9). This shows that the critical values of η_1 and η_2 increase with decreasing p. This dependence of a on evaporation is consistent with

[4]It should be mentioned that the non-zero value on η_1 is due to the rule that when a cell having m particles transfers to its q neighbours it transfers n to all of them subject to the maximum capacity N_0. We find $\eta_1 = 0$ if we impose the rule that the cell transfers m/q to all the neighbours. But this does not change the qualitative behavior of the dependence of exponent on evaporation.

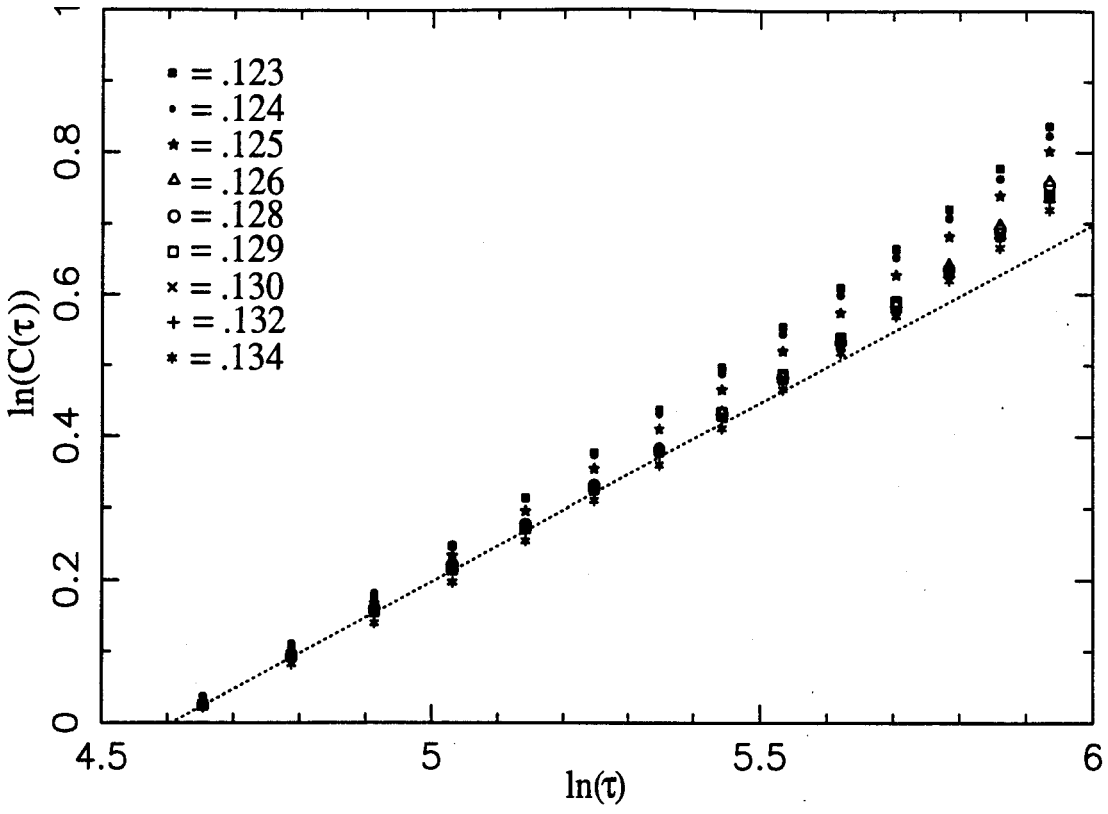

Figure 4.10: *The simulated time correlation function of height for various values of* η *and other parameters same as figure(4.6). The various symbols denote the values of* η*. The dotted line corresponds to a slope of 0.5.*

the experimental results described above.

In this model we can apply an external bias which could be present due to gravity or anisotropy in the medium. This bias was incorporated in the model by introducing a difference in the number of fluid particles transferred to the vertical and horizontal neighbours of a given cell. The different regimes described above were also observed in this case for a fixed value of η and p as the bias was varied.

In the model the fluid particles have more than one path to reach a particular cell. The effective number of paths available to reach a cell decreases as we increase evaporation. This is due to the fact that the increased evaporation suppresses the longer paths. For $\eta < \eta_1$, the number of fluid particles that a cell loses through evaporation is more than compensated by the inflow because of the many paths available, hence, in this regime the effective evaporation is zero and the values of exponents become greater than 0.5. As the number of paths become less, the particles get stuck at ob-

stacles for a longer time inducing a transition into a regime with exponents 0.5 [14]. On further increase of evaporation, the exponents becomes less than 0.5. In the case of biased random walk, this region is known to have exponents which change continuously with bias [19].

The dependence of the dynamical exponent β on evaporation is the same as that of α. In figure (4.10) we show the behavior of $C(\tau)$ for various values of η for a fixed value of p. We see that in regime I all the curves have a slope greater than 0.5. This slope changes continuously to 0.5 in regime II. In regime III, the slope decreases with η.

4.7.2 Internal Driving Force

The average number of particles in the wetting front can be considered as the reduced internal driving force f. In the model, we compute this internal driving force as follows. If N_i is the number of particles at i-th cell, then the average number in the front at any instant is defined as $\overline{N}(t) = \frac{1}{2L+1}\sum_{i=-L}^{L} N_i(t)$. Similarly, we define $\overline{N_c} = \frac{1}{2L+1}\sum_{i=-L}^{L} N_i(t \to \infty)$ as the average number of particles in the steady state. Then, the reduced internal driving force is defined as

$$f = \frac{\overline{N} - \overline{N_c}}{\overline{N_c}} \tag{4.7}$$

Evaporation continuously reduces this driving force. Depending on the behaviour of the driving force as a function of time, the growth behaviour of the interface also changes qualitatively.

To get an insight into the dependence of the roughness exponent a and saturated height-height correlation W_{sat} on the parameters mentioned above, we plot in figure ***(4.11)*** the change in reduced driving force f as a function of time [20]. It is shown that for the range of η considered f can be fitted to the following form

$$f(t) = B(\exp[A/(t + t_c)] - 1) \tag{4.8}$$

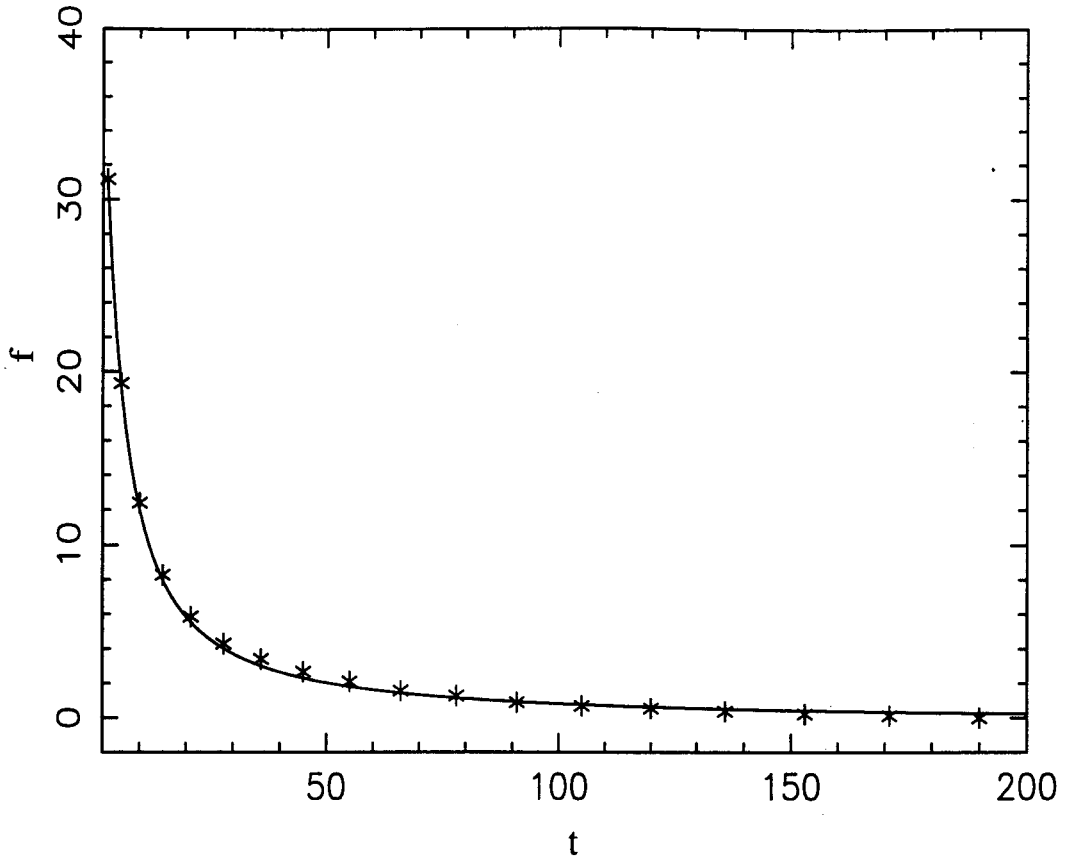

Figure 4.11: A plot of the reduced driving force f for $\eta = .136$, p = .45 and L = 6000. The continuous line is the fit to equation(4.8) with $t_c = 10.0$ and $A = 29.0$.

Here $A = A(\eta, \mathrm{p})$, $B(\eta, \mathrm{p})$, $t_c(\eta, \mathrm{p})$ are all functions of evaporation η and the blocking probability p. Changing p does not change the behaviour of f qualitatively but will change the values of A and t_c. This nonlinear dependence of f on time is certainly different from the DPD model in ref. [6]. This could be a reason for the change in the roughness exponent a, as a function of evaporation. However, more careful analysis is needed to establish this point.

The driving force f drops to a value f_s at t $\sim 2t_c$. This value f_s as a function of η is given in figure (4.12) at t $= 2t_c$. We would like to emphasize that changing η does not change t_c but merely changes the value of f_s at which the system is driven for a long time before it stops and A which sets the transient time scale. We find that there are two critical values of η, η_1 and η_2 at which the slope of the $f_s(\eta)$ curve changes drastically. The interface behaves differently in these three regions as discussed before. The static exponent a, can be computed when the driving force saturates. It was found that the exponent α (calculated at t $= 4t_c$) changes

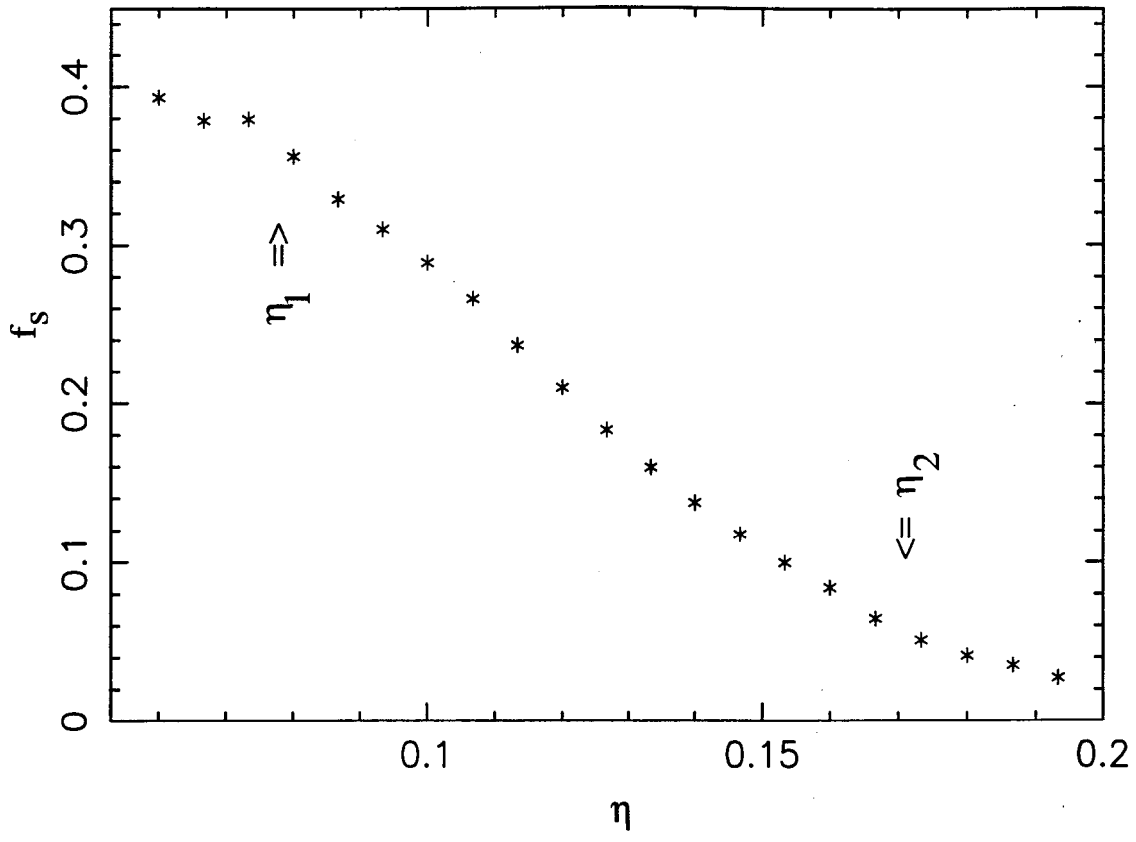

Figure *4.12: The reduced driving force* $f_s = f(2t_c)$ *showing two critical values of* η *for* $p = .45$. *The system size in this case is* ***6000.***

continuously with η.

4.7.3 Finite Size Scaling

In this section we perform a finite size scaling for a fixed value of evaporation η and p. In figure (4.13), we show the dependence of $W(l)$ on the system size L. We find that the saturated correlation W_{sat} of $W(l)$ depends on the system size as

$$W_{sat} \sim L^{\chi}, \tag{4.9}$$

with the correlation function $W(l, L)$ satisfying a finite size scaling form

$$W(l, L) = L^{\chi} g(l/L^{\nu}). \tag{4.10}$$

where $\chi = .34$ and $\nu = .68$ for $p = .2$ and $\eta = .293$ in regime II. The data collapse obtained with this scaling is shown in figure *(4.14).*

As implied by equations *(4.2)* and (4.10), we find the exponents χ, ν and a satisfies

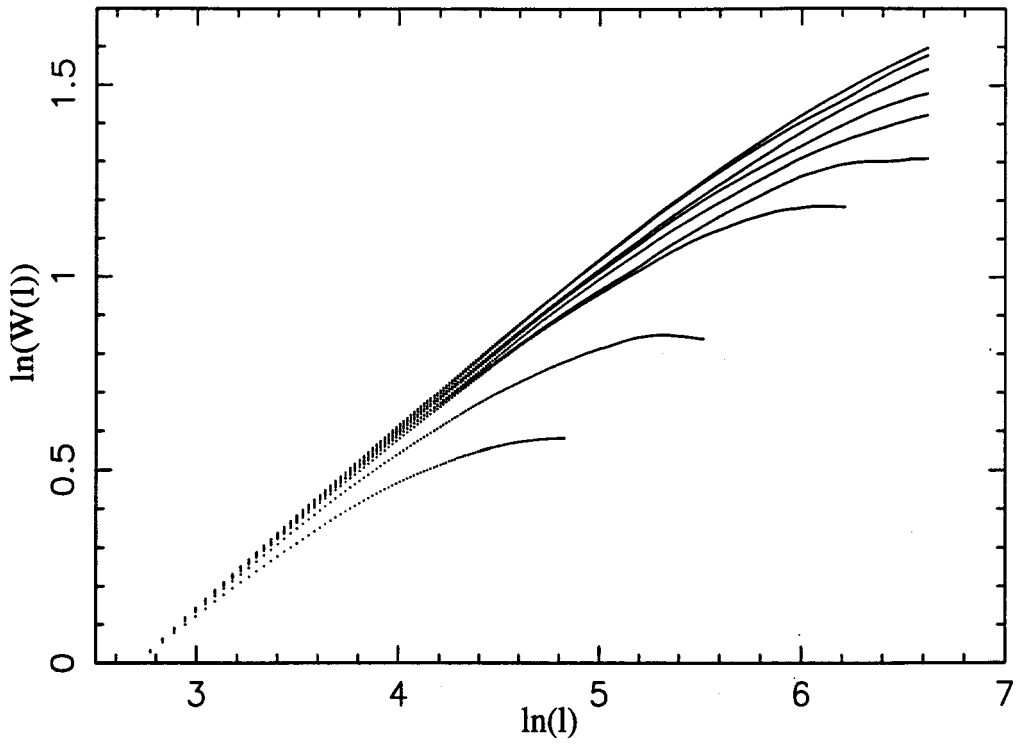

Figure 4.13: *The simulated height-height correlation function $W(l)$ plotted against the distance of separation l after the columns stopped growing for system sizes* $L =$ **125, 250, 500, 750, 1000, 1250, 1500, 1750, 2000** *from bottom,* $\mathbf{p} = \mathbf{.2}$, $\eta = .293$.

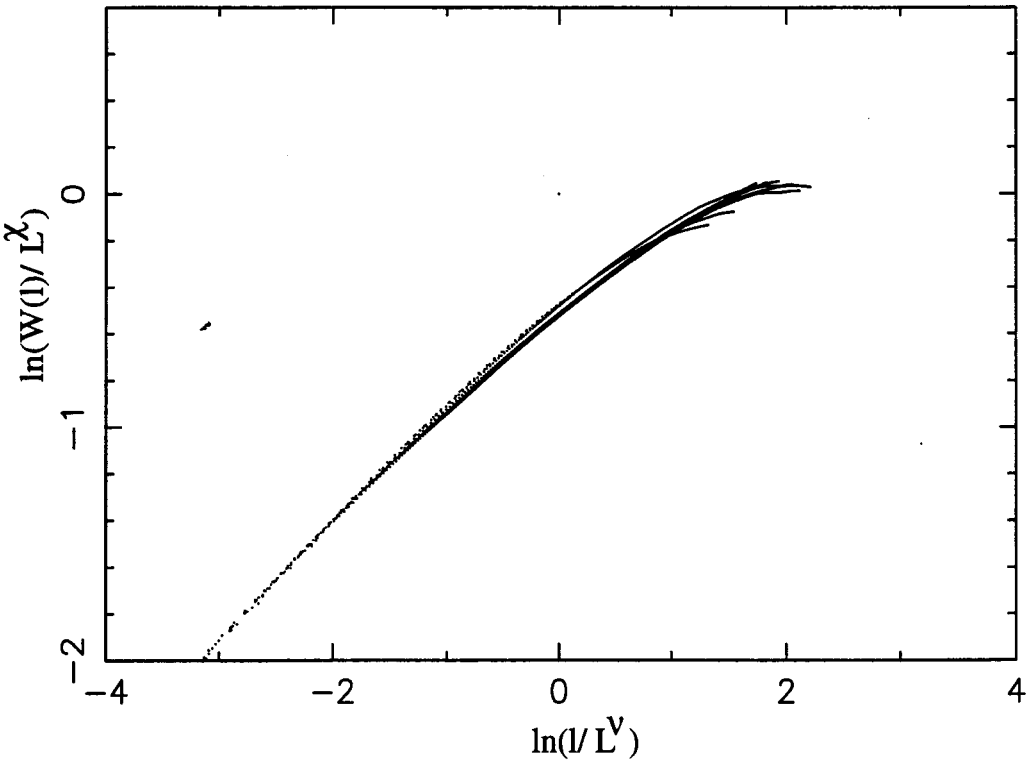

Figure 4.14: *The data collapse with the finite size scaling (see equation (4.10)) for* $\chi = \mathbf{.34}$ *and* $\nu = .68$. *The other parameters are same as figure (4.13).*

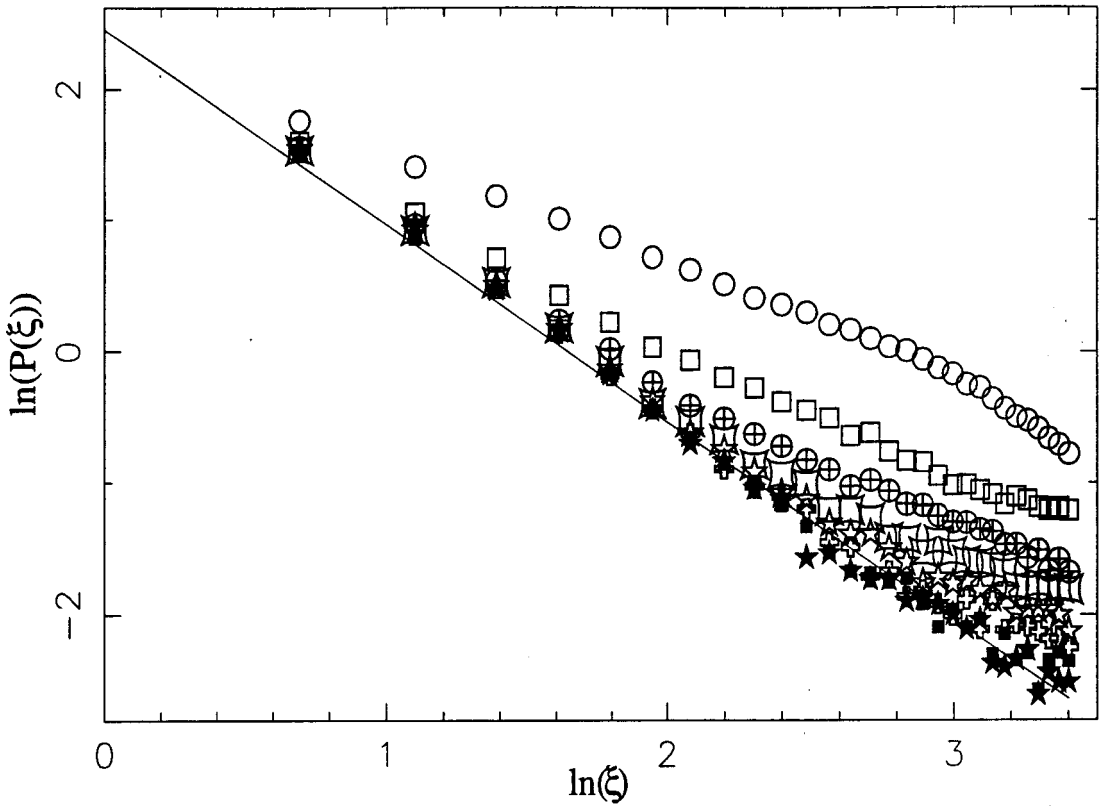

Figure 4.15: *Distribution of connected cluster of dry cells calculated at* $t = t_c$ *to* $t = 8t_c$. *Note that the distribution approaches to a power law given by* $P(\xi) \sim \xi^{-1.5}$. *The parameters are same as figure (4.11).*

the scaling relation [21]

$$\frac{\chi}{\nu} = \alpha, \tag{4.11}$$

since for the given value of p and η, $a = .52$. This system size scaling establishes that there is no single characteristic length scale in the problem. This implies that the function $W(l, \mathrm{L})$ obeys a power law relation given by equation (4.2) [21].

4.7.4 Distribution of Cluster of Dry Cells

It was mentioned earlier that the interface stops moving when all the boundary cells dry up. Thus, a connected cluster of dry cells is formed at the boundary. We show [20] in figure (4.15) that the length distribution of this connected clusters approaches a power law distribution,

$$P(\xi) \sim \xi^{-\kappa} \tag{4.12}$$

as $t \gg t_c$. This power law dependence is typical of scale invariant systems.

4.8 Self-organized Criticality (SOC)

In 1987, Bak, Tang and Wiesenfeld introduced the notion of self-organized criticality [22] in an investigation of extended dissipative dynamical systems. These dynamical systems naturally evolve into a "critical state" through a self-organization process. There is no external tuning parameter that must be adjusted to reach this critical state. This critical state is characterized by no intrinsic length or time scales. Bak, Tang and Wisenfeld suggested that sandpiles were a particularly clear example of a self-organized system. The grains are dropped onto a pile one by one, and the pile ultimately reaches a stationary critical state in which its slope fluctuates about a constant angle of repose. Each new grain added is capable of inducing an avalanche on any size scale.

Many models based on cellular automata have the property of self-organized criticality. The aim of this section is to study this self-organization process in interface growth. Even though there is a substantial amount of work in this field, till now there is no general agreement on the origin and characterization of SOC in different systems. In fact, conservation laws were believed to be necessary for the appearance of SOC [23]. However, there are also models which are nonconservative but still shows SOC [24, 25]. The model presented here belongs to this class of nonconservative systems exhibiting SOC. In our model it appears [20] that the rapid decay and subsequent *slow relaxation* of the driving force to zero is responsible for SOC.

As mentioned before, Sneppen [26] was the first to introduce a self-organized depinning (SOD) model. The main difference between the DPD model and SOD one is that SOD does not require a tunable driving force. Instead, the growth rules are enough to self-tune the interface to the critical point F_c - in this sense SOD model exemplifies the ideas of self-organized criticality. The scaling properties of SOD coincide with those of DPD model [27, 28]. To establish the SOC of the interface in our model, it is necessary to obtain the length and time distribution of avalanches

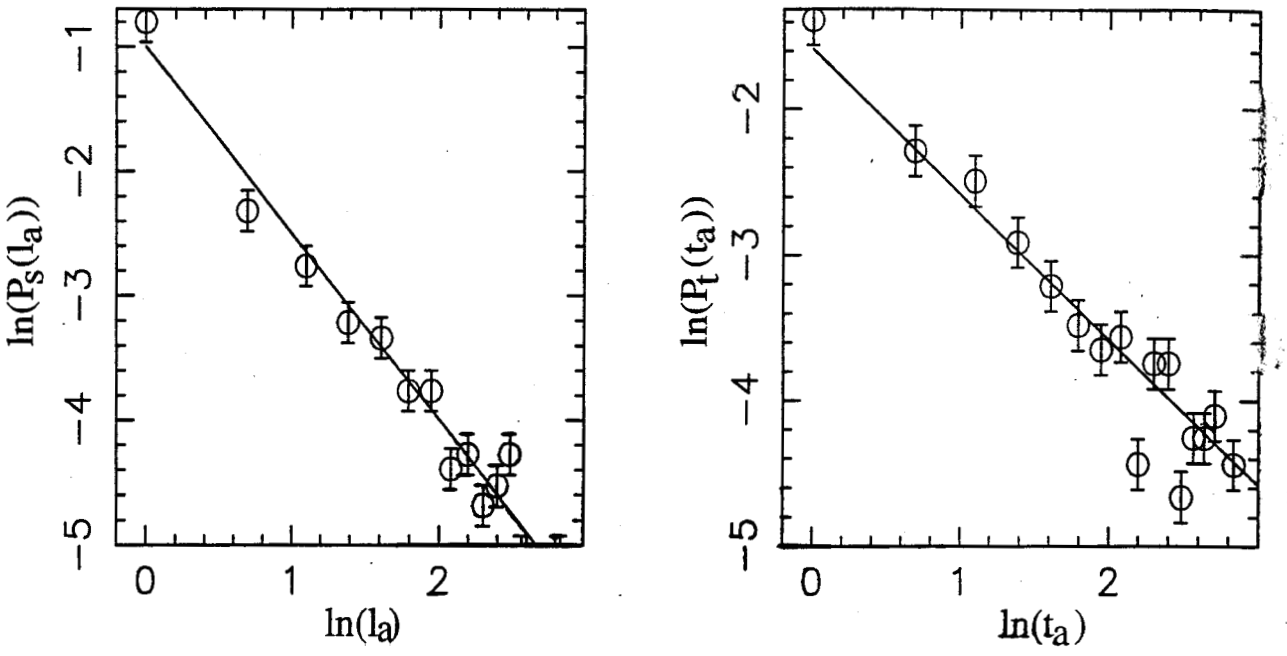

Figure 4.16: *Spatial and temporal distribution functions of the avalanches shown for the parameters same as in figure (4.11)*

[29]. When the interface stops moving, a connected cluster of dry cells is formed at the boundary. We then fill one of these *dry* cells with N_0 number of fluid particles. This results in further movement of the interface. This is motivated from the usual sandpile model in SOC where a grain of sand is added to study the resultant avalanches at all length scales. The distribution of spatial and temporal extents l, and t_a of these avalanches is shown in figure (4.16). These distributions are found to obey the power laws

$$P_s(l_a) \sim l_a^{-\kappa} \tag{4.13}$$

$$P_t(t_a) \sim t_a^{-\delta}, \tag{4.14}$$

where $P_s(l_a)$ is the frequency of occurrence of an avalanche of length l, and $P_t(t_a)$ is the frequency of occurrence of an avalanche lasting a time t_a. The exponent δ has a universal value equal to 1.0 for $\eta_1 < \eta < \eta_2$. It has been argued recently by Boer *et al.* that the mere existence of power law correlations is not sufficient to establish SOC [29]. They take the non-normalizability of the temporal distribution function to be the criterion of SOC. The corresponding argument here is the following. For an infinite lattice, the finiteness of the integral $\int_1^\infty P(t_a)dt_a$ means that points infinitely

far from the origin of avalanche do not participate in the avalanche process. If the interface is critical, it is robust against any disturbance; *i.e.* an avalanche should leave the interface unchanged. This is possible only if all the points on the interface has a nonzero probability of participating in the avalanche indicating $P(t_a)$ as $t_a \to \infty$ to be significant. This results in the divergence of the integral. The value of $\delta = 1.0$ in our simulation satisfies this criterion establishing the SOC of the interface. There exists a simple relation between the exponents κ and α given by $\kappa = 1.0 + \alpha$. This can be seen from the following. The total area covered by an avalanche of size l_a is $\int_0^{l_a} l_a^{\alpha} dl_a \sim l_a^{1+\alpha}$. Since the probability of finding a blocked site is uniform, the probability of the avalanche of size l_a is $l_a^{-(1+\alpha)}$. The same argument applies for the distribution $P(\xi)$ shown in figure (4.15). To understand this critical behaviour of the interface we examine the form of the driving force. Note that (see figure (4.11)) the time dependence of the driving force is of the form given in equation (4.8). This means that the interface is driven by a force $\mathbf{F} \sim F_c$ for a long time. It should be noted that the tuning of the driving force to F_c is done by the system internally. This is a characteristic feature of self organizing systems, wherein the system is driven in a region close to criticality by itself [30]. This shows that in this region of η the interface exhibits self-organization. It is now quite established [31] that this type of slow driving force underlies most (if not all) models of SOC.

4.9 Multi-affinity

As mentioned earlier, the self-affine interfaces are invariant under an anisotropic scale change. This self-affine interface is characterized by a single exponent. In this section, we demonstrate that the scaling properties of the interface generated from our model is described by an infinite set of exponents and thus the model obeys multi-affine scaling. In other words, higher moments of height-height correlation do not scale with the same exponents. In the context of interface growth, the concept

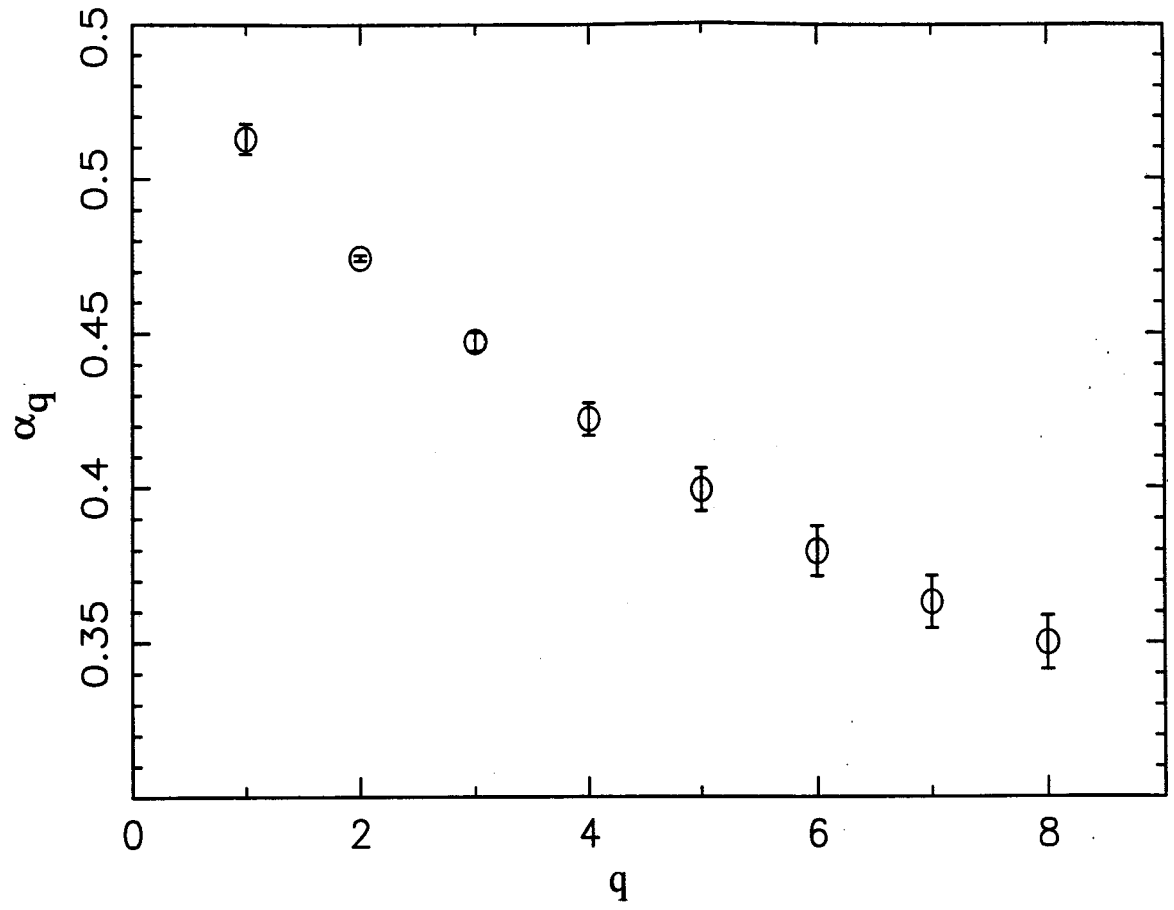

Figure *4.17: The exponent a, has been plotted against q. Parameters are* $p = .45$, $\eta = .136$ *and* $L = 6000$.

of multi-affinity was first introduced by Barabási et. al. [32]. To check for this multi-scaling of the interface, one has to compute the exponents of the q-th order height-height correlation function defined by

$$c_q(l) = \langle |h(x+l) - h(x)|^q \rangle_x \tag{4.15}$$

Numerical simulation shows that $c_q(l) \sim l^{q\alpha_q}$. Notice that $c_2(l)$ is related to the height-height correlation function W(l) defined in equation *(4.1)* by $c_2(l) = [W(l)]^2$.

In the model simulation [32] of the evolution of height variable $h(x,t)$ in (1+1) dimensions with power law distributed noise [5] , it was shown that exponents a, *decrease* with *q.* It was also noticed [32] that the exponents change with the order q continuously with a sharp change of the exponents at q $\sim$ *3* indicating a phase transition.

[5] Starting from a flat surface h = 0 at $t = 0$, the system evolves up to time t, performing t times the following rules. (a) The noise $\zeta(x,t)$ is added to every site; (b) each site takes a new value $h(x,t+1)$ equal to the maximum of itself and its two nearest neighbours. The noise ζ was taken from a power-law distribution of the form $P(\zeta) \sim \zeta^{-(1+\mu)}$ for $\zeta > 1$ and $P(\zeta) = 0$ otherwise.

Here, we study [20] the q-th order correlation function of height differences in our model. In our computation of $c_q(l)$, only positive moments are considered. They indicate the multi-affinity of the interface if $a_q \neq constant$ for all values of q.

The exponents a_q for various values of q are shown in figure (4.17). As is well known for multi-affine surfaces, we find α_q to change *continuously* with q. Thus, this variation of a_q with q strongly suggests that the distribution of height differences is **multi-affine**. It is evident from the figure (4.17) that a_q is a *decreasing* function of *q*. It is interesting to note in this connection that for a continuous Brownian motion, the exponent $a_q = 1/2$ for all positive values of q. Even the Lorentzian and exponential distributions fall into this self-affine class having $a_q = 1$ for all positive values of q.

There is another way for displaying the set of infinite exponents. This method is common in statistical as well as disordered electronic systems. We carry out this multi-fractal analysis using the height distribution $N(j)$ [33, 34]. Here, j is the deviation of height of the columns from the mean h. We define a normalized probability distribution

$$P(j) = \frac{N(j)}{\sum_{k=-M}^{M} N(k)} \tag{4.16}$$

and its m-th power $W_m(j)$ as

$$W_m(j) = \frac{P(j)^m}{\sum_{k=-M}^{M} P(k)^m}$$

Then, the singularity spectrum f (8) is defined[6] as

$$f_m = \frac{-1}{\ln(2M+1)} \sum_{k=-M}^{M} W_m(k) \ln W_m(k) \tag{4.17}$$

and

$$\theta_m = \frac{-1}{\ln(2M+1)} \sum_{k=-M}^{M} \ln W_m(k). \tag{4.18}$$

[6] In this definition, both positive and negative values of *m* (including zero) have been considered. This has been depicted in figure (4.18) explicitly.

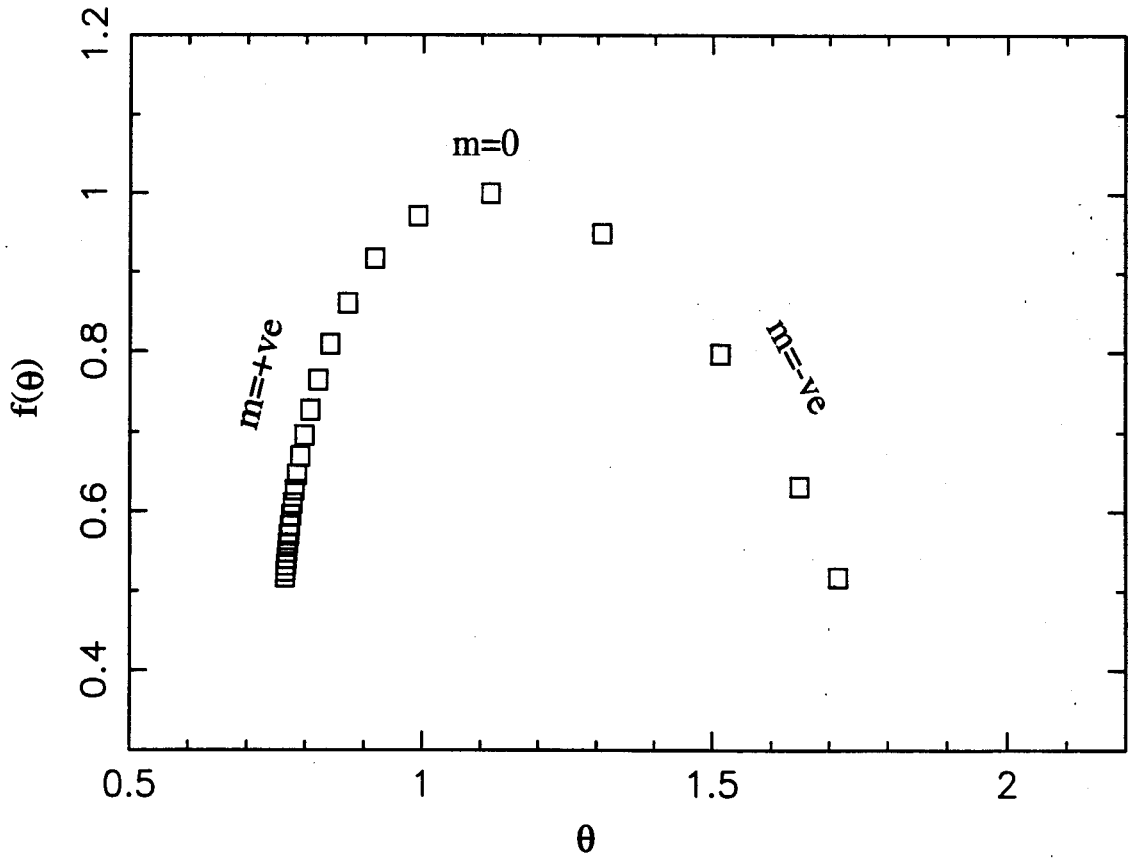

Figure **4.18:** f **(8)** *versus* **8** *spectrum for the same parameters as figure (4.17).*

Equations **(4.17)** and **(4.18)** define a function $f(\theta)$ parametrically, where m is the parameter. In figure (4.18), we depict the smooth dependence of f **(8)** on **8.** Note that for ordinary fractals, f **(8)** is a constant. For multi-affine fractals, $f(\theta)$ is **as** shown in figure **(4.18).**

4.10 Cornparision with KPZ and DPD Models

A crossover of a from **.63** to 0.5 is seen in the **DPD** model [9]. However, the dependence of the exponents on evaporation seen in the present model is different from this crossover. This is supported by the following arguments.

1. In both simulation and experiment, we find the exponent a to vary from a value below 0.5 (KPZ) to one above 0.63 **(DPD).**

2. The dynamic exponent β obtained from the simulation is not the same as the KPZ value in the region where $a = 0.5$.

3. Unlike the crossover region observed in DPD models, here the exponents'are measured only after the growth stops by forming a cluster of dry cells at the interface.

4. KPZ type of behaviour is expected when the interface is moving with a constant velocity, like driving DPD model with p $< p_c$. But in the present model even though p $< p_c$, evaporation continuously decreases the velocity to zero.

These points show that the underlying physics here is different from that of the DPD and KPZ models. Another two interesting points which distinguish the present model from DPD model are the following. (i) the DP model is driven to p_c linearly whereas the present model has a nonlinear driving force leading to the stoppage of the interface growth and most importantly (ii) we find the avalanches to show a power law distribution within a range of evaporation while the avalanches in the DPD model shows no interesting scaling behaviour and has an exponential distribution [28]. This power law distribution shows that evaporation does not set any length scale in contrast to the DPD model wherein there is a length scale set by the value of Ap. In Appendix B, we present a comparative study of the exponents obtained in various models and experiments.

4.11 Conclusion

It is to be noted that the results are presented for a particular choice of parameters in the model. A change in the parameters does not alter the gross features. The main points of this chapter can be summarized as follows.

(i) We have shown from experiments conducted at two different conditions that the exponent a in imbibition is not the same as obtained in previous experiments.

(ii) **A** model for imbibition which includes the effect of evaporation through loss of fluid particles on transfer is presented.

(iii) The model shows that the static height - height correlation exponent a depends on the evaporation which is partly consistent with our experiments.

(iv) The interface is shown to exhibit power law distribution of avalanches for a region of evaporation.

(v) It is shown that the driving force tunes itself close to the critical value for all values of evaporation $\eta_1 < \eta < \eta_2$. This slow driving of the system close to pinning can be understood **as** the reason for the existence of a power law distribution of avalanches.

(vi) The interface also shows multi-affinity.

To conclude, imbibition experiments show that the roughness exponents depend on evaporation. **A** first principles cellular automaton model for imbibition gives results in qualitative agreement with experiments. Also the model exhibits properties much richer than the already known models of imbibition.

Bibliography

[1] J. Krug, Adv. Phys, 46, 139 (1997).

[2] T. H. Healy and Y. -C. Zhang, Physics Reports., 254, 215 (1995).

[3] A. L. Barabási and H. E. Stanley, *Fractal Concepts in Surface Growth* (Cambridge University Press, Cambridge, England, (1991).

[4] T. Vicsek, *Fractal Growth Phenomena* (World Scientific, Singapore. 1992), 2nd ed., Pt IV; *Solids Far From Equilibrium: Growth, Morphology and defects*, edited by C.Godreche (Cambridge University Press, Cambridge, England, (1991).

[5] J.W. Evans, Rev. Mod. Phys., 65, 1281 (1993).

[6] L.A.N. Amaral, A.L. Barabási, S.V. Buldyrev, S. Havlin and H.E. Stanley, Phys. Rev. Lett., 72, 641 (1994), L.A.N. Arnaral, A.L. Barabási, S.V. Buldyrev, S.T. Harrington, S. Havlin, R. Sadr-Lahijany, and H.E. Stanley, Phys. Rev. E 51, 4655 (1995).

[7] *Random Fluctuations and pattern growth: Experiments and Models*, edited by H.E. Stanley and N. Ostrowsky, NATO ASI Series E:Vol 157, (Kluwer Academic Publishers, 1988).

[8] M.C. Cross and P.C. Hohenberg, Rev. Mod. Phys., 65, 851 (1993).

[9] A.L. Barabási, S.V. Buldyrev, S. Havlin, G. Huber, H.E. Stanley and T. Vicsek, in *Surface Disordering: Growth, Roughening and Phase Transitions* edited by

R. Jullien, J. Kertsez, P. Meakin and D.E. Wolf, Proceedings of the Les Houches Workshop, 1992 (Nova Science, New York, 1992), L.H. Tang and H. Leschhorn, Phys. Rev. A., 45, R8309 (1992), S.V. Buldyrev, A.-L. Barabási, F. Caserta, S. Havlin, H.E. Stanley and T. Vicsek, Phys. Rev. A., 45, R8313 (1992).

[10] Fractals and Disordered Systems edited by A. Bunde and S. Havlin, (Springer-Verlag, Berlin, 1991).

[11] K. Sneppen, Phys. Rev. Lett., 69, 3539 (1992).

[12] P.B. Sunil Kumar and Debnarayan Jana, Proceedings of "Dynamics of Complex systems", Satellite meeting to STATPHYS-19 (1995). Physica A, 224, 199 (1996).

[13] T. H. Kwon, A. E. Hopkins and S. E. O'Donnell, Phys. Rev. E., 54,685 (1996).

[14] M. Kardar, G. Parisi and Y.-C. Zhang, Phys. Rev. Lett., 56, 889 (1986).

[15] F. Family, K. C. B. Chan and J. Amar, 'Dynamics of interface roughening in imbibition' in Surface Disordering: Growth, Roughening and Phase Transitions, edited by R. Jullien, J. Kertész, P. Meakin and D. E. Wolf (Nova Science, New York, 1992).

[16] S. F. Edwards and D. R. Wilkinson, Proc. Roy. Soc. London, A381, 17 (1982).

[17] J. M. Kim and J. M. Kosterlitz, Phys. Rev. Lett., 62, 2289 (1989).

[18] M.Eden, in Symposium on Information Theory in Biology, H. P. Yockey, ed. (pergamon Press, New York, 1958); Also, in Proc. Fourth Berkeley Symposium on Mathematical Statistics and Probability, F. Neyman. ed., vol. IV (UC-Berkeley, 1961).

[19] S. Havlin and D. Ben-Avraham, Adv. Phys. 36, 695 (1987).

[20] P. B. Sunil Kumar and Debnarayan Jana (Unpublished).

[21] L.P. Kadanoff, S.R.. Nagel, L. Wu and S. Zhou, Phys. Rev. A, 39, 6524 (1989).

[22] P. Bak, C. Tang and K. Wiesenfeld, Phys. Rev. Lett. 59, 381 (1987); Phys. Rev. A, 38, 364 (1988).

[23] G. Grienstein, D.-H. Lee and S. Sachdev, Phys. Rev. Lett. 64, 1927 (1990).

[24] Z. Olami, H.J.S. Feder and K. Christensen, Phys. Rev. Lett., 68, 1244 (1992), K. Christensen and Z. Olami, Phys. Rev. A, 46, 1829 (1992).

[25] A.A. Middleton and Chao Tang, Phys. Rev. Lett. 74, 742 (1995).

[26] K. Sneppen, Phys. Rev. Lett., 69, 3539 (1992); K. Sneppen and M. H. Jensen, Phys. Rev. Lett., **71,** 101 (1993).

[27] H. Leschhorn and L.-H. Tang, Phys. Rev. E, 49, 1238 (1994).

[28] Z. Olami, I. Procaccia and R. Zeitak, Phys. Rev. E., 49, 1232 (1994).

[29] J. de Boer, A.D. Jackson and Tilo Wettig, Phys. Rev. E, 51, 1059 (1995).

[30] D. Sornette, A. Johansen and I. Dornic, J. Phys. I France 5, 325 (1995).

[31] M. Marsili, G. Caldarelli and M. Vendruscolo, Phys. Rev. E, 53, R13 (1996).

[32] A.-L. Barabasi and T. Vicsek, Phys. Rev. A, 44, 2730 (1991); A.-L. Barabasi, R. Bourbonnais, M. Jensen, J. Kertész, T. Vicsek and Y.-C. Zhang, Phys. Rev. A, 45, R6951 (1992).

[33] T.C. Halsey, M.H. Jensen, L.P. Kadanoff, I. Procaccia, and B.I. Shraiman, Phy. Rev. A. 33, 1141 (1986).

[34] P.K. Thakur and C. Basu, Physica A, 216, 45 (1995).